THE ASTROPHYSICAL JOURNAL, 307:302–312, 1986 August 1

VLA MAPS OF FORMALDEHYDE ABSORPTION TOWARD NGC 2024

RICHARD M. CRUTCHER
Astronomy Department, University of Illinois

C. HENKEL AND T. L. WILSON
Max-Planck-Institut für Radioastronomie, Bonn

K. J. JOHNSTON
E. O. Hulburt Center for Space Research, Naval Research Laboratory, Washington, DC

AND

J. H. BIEGING
Radio Astronomy Laboratory, University of California, Berkeley
Received 1985 May 13; accepted 1986 January 10

ABSTRACT

VLA[1] continuum and H_2CO absorption line mapping observations at 6 cm wavelength of the H II region/molecular cloud NGC 2024 are presented. The angular and velocity resolutions are 13″.8 × 12″.8 (P.A. 77°) and 0.4 km s^{-1}. The continuum map shows two partially resolved, compact peaks along a north-south line. There are lower intensity filaments stretching east-west and then northward from the northern peak. The total flux density in the map is 24 Jy, which is 43% of the single-dish flux density. The distribution of the 1_{10}–1_{11} absorption line of H_2CO follows the dark optical dust lane. Toward the more intense continuum regions, the maximum apparent optical depth is ~1 or less. As noted previously, the velocity of the deepest H_2CO absorption is ~1 km s^{-1} more negative than velocities of high-excitation millimeter wavelength lines. From the median optical depth, other H_2CO results and a model, we estimate that the corrected ($H_2CO/H_2{}^{13}CO$) ratio is ~70 and the H_2 density is $10^{4.9}$ cm^{-3}. Our observations and other results lead us to formulate a model of NGC 2024: A bubble has been blown in the molecular cloud by a newly formed star (or stars). The (as yet undetected) principal ionizing star is probably near the peak of the southern compact H II region and the unresolved ionization front at the southern edge of the radio continuum map. Photons from this star penetrate the dense molecular gas to the south, producing both strong extended infrared emission just south of the ionization front and strong carbon recombination-line emission. Ionized hydrogen flows northward from this ionization front into the cavity of the molecular bubble. This flow apparently interacts with a stellar wind from the bright infrared point source IRS 2, leading to a concentration of H II at the northern continuum peak. The H II flows around IRS 2 and escapes from the cavity through the molecular bubble.

Subject headings: interstellar: molecules — nebulae: H II regions — nebulae: individual

I. INTRODUCTION

The H II region and associated molecular cloud NGC 2024 (Orion B, W12) have been the subject of a number of detailed spectroscopic and continuum observational studies at both infrared and radio wavelengths. These have included searches for 2 μm point sources (Grasdalen 1974), infrared spectroscopy of the brightest point sources (Thompson, Thronson, and Campbell 1981; Crutcher and Hall 1983; Black and Willner 1984), mapping of extended infrared emission from 8 to 200 μm (Grasdalen 1974; Frey *et al.* 1979; Thronson *et al.* 1984), mapping of millimeter-wavelength molecular emission lines (Snell *et al.* 1983; Thronson *et al.* 1984), of centimeter-wavelength absorption lines (Bieging, Wilson, and Downes 1982), and of 76α recombination lines (Krügel *et al.* 1982). Many of these studies have included the formulation of models of the H II region/molecular cloud. However, a major deficiency in the observational data base is a high-quality, high angular resolution synthesis map of the radio continuum and molecular lines.

We have carried out an aperture-synthesis mapping study of the 6 cm absorption line of H_2CO and of the continuum of NGC 2024. In this paper we report the results of these observations. The new data show details and features of the H II region and molecular gas which were not previously known and, together with the published data, allow the formulation of a more comprehensive and accurate model of the region. The optical depth of the 6 cm H_2CO, together with 2 cm H_2CO line data, is used to estimate the average H_2 density. Photon trapping corrections for the ($H_2{}^{12}CO/H_2{}^{13}CO$) ratio are estimated from these data.

II. OBSERVATIONS

Aperture synthesis maps of NGC 2024 in the 1_{10}–1_{11} line of H_2CO at 4.82966 GHz were made with the Very Large Array (VLA) of the National Radio Astronomy Observatory[2] in the D configuration on 1982 December 1. A total of 18 antennas were used with a maximum baseline of 1.0 km. Spectra of 31 channels spaced by 0.38 km s^{-1} with a resolution of 0.46 km s^{-1} were obtained. The center of the spectral window was at 10 km s^{-1}. Every 20 minutes the local oscillator setting was updated for Doppler tracking; hence, radial velocities are accu-

[1] The VLA is a facility of the National Radio Astronomy Observatory, which is operated by Associated Universities, Inc., under contract with the National Science Foundation.

[2] The National Radio Astronomy Observatory is operated by Associated Universities, Inc., under contract with the National Science Foundation.

rate to 0.03 km s^{-1}. The phase center of the array was α_{1950} = $05^h39^m15^s$, $\delta_{1950} = -01°55'00''$. The primary flux calibrator was 3C 286, for which a flux of 7.46 Jy was assumed. We monitored the calibrator 0539–057 every half hour for 5^m and derived a flux of (1.166 ± 0.012) Jy. A continuum visibility data set was formed by averaging the visibility data for the nine channels at each end of the spectrum which showed no evidence for H_2CO absorption. The untapered continuum and line visibility data were natural weighted before Fourier transforming. Maps were also made with a taper of 15 kλ; only minor differences at the lowest contour level were seen.

The visibility records were self-calibrated in phase. The clean components of the continuum map were used as the input model for self-calibration of the visibility phases of the continuum data. A new continuum map was then computed and cleaned to a level of 5 mJy. Subsequently, the phase corrections determined by the self-calibration procedure were applied to the visibility records of each spectral-line channel. These visibility records were then Fourier transformed and cleaned to the same level as the continuum map. The continuum channel was then subtracted from the line maps. The 1 σ noise level of these channel maps was ~10 mJy per beam (= 3.0 K main beam brightness temperature). There are negative sidelobes up to 30 mJy per beam. The beam of the cleaned map is 13″8 × 12″8, P.A. 77°.

The H_2CO maps of optical depth were computed from the cleaned continuum map and the individual cleaned line-channel maps. Because of signal-to-noise considerations, the H_2CO optical depths were computed only over the area where the continuum level was at least 10% of the peak continuum intensity of 0.63 Jy per beam. The adopted cutoff means that at the edge of the maps, a 1 σ noise uncertainty implies that an actual optical depth of 0 may appear in a single pixel as an optical depth of about ±0.2. The same optical depth uncertainty at positions near the continuum peaks is 0.02. The intensity level over the map should be raised by 60 mJy beam^{-1} (see our discussion in § III*b*). Hence, the apparent optical depths at the edges of the maps could be a factor of 2 lower than shown. The line spectra, to be discussed in § III*e* and shown in Figure 2, were obtained from the maps tapered to 15 kλ.

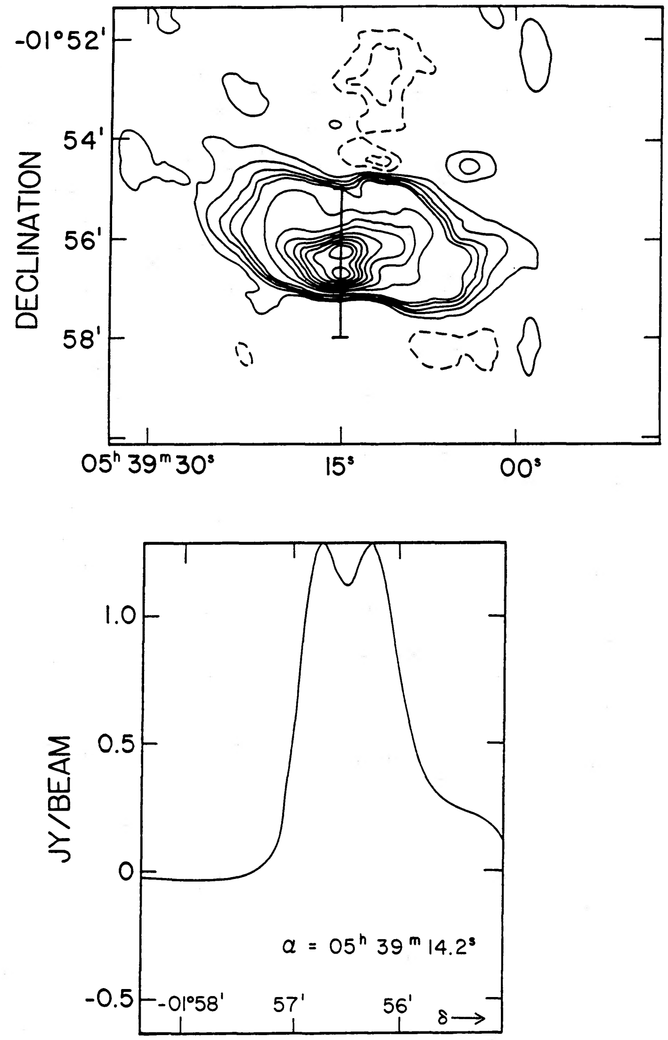

FIG. 1.—(*a*) A map of the continuum emission toward NGC 2024 and (*b*) a cut in declination through the northern and southern continuum peaks denoted by "NCP" and "SCP", respectively.

III. RESULTS AND DISCUSSION

a) VLA Continuum Data

The continuum map is shown in Figure 1*a*. The total cleaned flux density of the continuum map is 24 Jy, which is 43% of the total flux density, 56 ± 4 Jy of the source (see, e.g., Krügel *et al.* 1982 and references therein). Hence, even in the D-array, at 6 cm NGC 2024 is partially resolved by the shortest spacings of the VLA. At the assumed 450 pc distance of NGC 2024, the scale is 15″ = 10^{17} cm. Contours are labeled as percentages of 600 mJy (=180 K, main beam T_B). There are two maxima of equal intensity. From Figure 1*a* these peaks appear to define the positions of two compact and partially resolved regions within the more extended continuum emission. Both peaks have the same right ascension, $\alpha_{1950} = 05^h39^m14^s.2$. The declinations of the two peaks are $\delta_{1950} = -01°56'42''$ and $-01°56'17''$. We show the distribution of continuum intensities along the north-south direction through the continuum peaks in Figure 1*b*. We shall subsequently refer to these peaks as the southern compact peak (SCP) and the northern compact peak (NCP). The SCP is resolved in the east-west direction, where its measured full width to half-power (FWHP) is 60″. To the south of the SCP the contours are consistent with an unresolved edge. To the north the SCP may be slightly extended. A definite statement cannot be made because of blending. The NCP is considerably broader than the SCP in the east-west direction, with a deconvolved FWHP of ~105″. In the north-south direction, emission from the NCP is extended to the N and blended with the SCP in the south. About 20″ north of the NCP, the emission blends into the more extended continuum. To the north of the NCP the contours resemble "crab claws" which are symmetric on a N-S line. This symmetry breaks down at roughly the 20% contour, where the ridge extending to the west bifurcates, with one ridge line turning northward to a north-south alignment while the other extends to the southwest. To the east of the NCP, a somewhat similar morphology is found. The extent to the east is smaller than to the west, and there is no bifurcation.

b) Other High-Resolution Continuum Maps and Missing Flux Density

The map of Krügel *et al.* (1982), made with a 1′ beam at 2 cm contains a total flux density of 56 Jy and covers a region 9′.7

$\times$ 8$'$.6 ($\alpha \times \delta$), to a contour level 2% of the peak. The deconvolved FWHP of the peak of Krügel *et al.* (1982) is 3$'$.1 $\times$ 1$'$.7 ($\alpha \times \delta$). Since the H II region is presumably optically thin at these wavelengths, our map misses the 32 Jy from the extended regions. In the map of Krügel *et al.* 1982, our two peaks are blended into one maximum by the larger beam. The average position of our two peaks agrees fairly well with the center of the 2 cm map. In order to estimate the flux per beam which is resolved out of our VLA map, we have subtracted the continuum response in our map from the map of Krügel *et al.* (1982). The continuum flux which remains is consistent with a uniform flux density of ~60 mJy per VLA beam (~18 K main beam brightness temperature) over about a 5$'$.5 $\times$ 3$'$.7 ($\alpha \times \delta$) area. The 21 cm synthesis map of Löbert and Goss (1978) has maxima at $\alpha_{1950} = 05^h39^m09^s.8$, $\delta_{1950} = -01°55'43''$ and $\alpha_{1950} = 05^h39^m13^s.2$, $\delta_{1950} = -01°56'28''$ (1950.0). The first peak is not present as a discrete source on our map; there is, however, a shoulder in this direction (see Fig. 1*a*). The peak T_B in our map is 20% lower than predicted on the basis of an extended, optically thin feature. The second peak listed by Löbert and Goss (1978) is 12$''$ west of the average position of our two peaks and is presumably a blend of these. The total flux density quoted by Löbert and Goss (1978) is 17% larger than that of Krügel *et al.* (1982), which is consistent with an optically thin H II region between wavelengths of 2 and 21 cm.

c) Comparison of the Continuum Map with IR Results

Grasdalen (1974) surveyed the area at 2 μm for infrared point sources and discovered a new infrared source, which at wavelengths longward of 2 μm is the brightest source in the area. Comparison of infrared color excesses at 5 μm or less led to the result that the reddening to the source (IRS 2) is 3.9 times larger than the reddening to IRS 1, a visible B0.5 Vp star with $E(B-V) = 1.7$ (Garrison 1968). IRS 2 is located 22$''$ north of the NCP; there is no evidence in our data for a local enhancement of the radio continuum at the IRS 2 position.

Thompson, Thronson, and Campbell (1981) obtained spectra at 2 μm with a spectral resolution of 3×10^3 of IRS 1, IRS 2, and several surrounding positions. They found strong Brackett series emission lines of hydrogen at the position of IRS 2 and much weaker Bγ emission lines towards IRS 1 and 15$''$ south of IRS 2; no line emission was detected 15$''$ north, east, or west of IRS 2. With the assumption that the Bγ through B14 lines observed toward IRS 2 had the intrinsic relative strengths given by Menzel's recombination case B, they derived $A_v = 12 \pm 3$ mag for the extinction toward IRS 2. If so, the luminosity of IRS 2, $1 \times 10^4 L_\odot$, is at least a factor of 5 less than the luminosity of the H II region. Our continuum map shows *no* peak within 10$''$ of IRS 2. These data strengthen the argument (Thompson *et al.* 1981) that the exciting star is not IRS 2 but instead lies in the SCP.

What is IRS 2? The Brackett lines (Crutcher and Hall 1983; Black and Willner 1984) show a FWHP of 150 km s^{-1} and a full width to zero power of 500 km s^{-1}. These results seem to indicate a large outflow from IRS 2. Using the formalism of Simon *et al.* (1983), we find $\dot{M}$ for IRS 2 to be $\sim 4 \times 10^{-7} M_\odot$ yr^{-1}, and it may be similar to the BN object in Orion-KL. Thompson *et al.* (1981) suggested that the exciting star is heavily embedded in dust and hence has remained undiscovered. Subsequently, we shall refer to this hypothesized dominant ionizing star as S3; if it is eventually detected as an infrared point source, the natural designation with be IRS 3.

Maps of extended infrared emission from NGC 2024 have been made at wavelengths of 8.4 μm (Grasdalen 1974) and at 40, 60, 100, 160, and 200 μm (Thronson *et al.* 1984). All of the extended infrared emission peaks at the same position, which is ~17$''$ to the southwest of the SCP (Fig. 1*a*). The distribution of the 8.4 μm emission is very elongated east-west. At longer wavelengths the distribution of the emission becomes more circular.

d) Radio Recombination Lines

Krügel *et al.* (1982) reported that the electron temperature, T_e, has a maximum of 9500 K just southwest of the position of the SCP seen on the VLA map (within the positional uncertainty, this peak could agree with the SCP position). With some small-scale deviations, the electron temperature decreases monotonically to the north by ~1000 K per arc minute. The LSR radial velocity of the H II is ~7 km s^{-1} at the position of the SCP (Krügel *et al.* 1982). This is not quite the maximum radial velocity, which is 9 km s^{-1} and occurs ~2$'$ west of the SCP. The radial velocities decrease toward the north-northwest by ~1.7 km s^{-1} per arc minute, reaching values of ~0 km s^{-1} at ~4$'$ north of the SCP. The C76α emission is strongly concentrated near or just south of the SCP. The He/H recombination-line strength ratios are ~0.02. Thompson *et al.* (1981) and Krügel *et al.* (1982) have argued that this low apparent He/H ratio was caused by the relatively low temperature of the principal ionizing star and used that ratio to estimate the spectral type of the exciting star as O9.

e) H_2CO *Absorption Line Maps: Morphology*

We first examine the line maps, formed by subtracting the continuum map from the maps at each channel which contains absorption. The absorption lines appear to have maxima at the two continuum peaks; to the west of the continuum peaks at $\sim\alpha_{1950} = 5^h39^m09^s.50$, $\delta_{1950} = -01°56'08''$; and to the north of the continuum peaks at $\alpha_{1950} = 5^h39^m12^s.73$, $\delta_{1950} = 01°55'02''$. Spectra toward these sources, another position close to the southern edge of the continuum, and the overall absorption spectrum are displayed in Figure 2. The spectral feature at 12.5 km s^{-1} appears to be associated only with the western continuum peak. There is also a trend for the line absorption peak to become more positive by 0.3 km s^{-1} arcmin^{-1} going from the south edge of the continuum to the northern features.

From sensitivity limitations, the H_2CO absorption measured with the VLA samples only that molecular gas in front of the continuum source, while single-dish results can also sample molecular gas which absorbs the 2.7 K background and which is behind the H II region. At the velocity of maximum absorption, 9.3 km s^{-1}, our line absorption flux density integrated over the continuum region is 4.8 Jy, or 72% of the corresponding single-dish value. The missing 28% of the line flux density could be from H_2CO located either in smooth, extended low surface brightness gas in front of the continuum source or in gas behind the H II region. In the first case, the optical depth in the H_2CO line will be small; in the second case, it must be large. We can rule out the possibility that most or all of the missing line flux density is caused by H_2CO which is behind the continuum source and very optically thick in the 6 cm line, since the molecular gas behind the continuum source has a radial velocity which is ~1.2 km s^{-1} higher than that in front and no significant contribution to the single-dish line flux at the more positive velocity is found in the profiles presented by Henkel, Wilson, and Bieging (1982).

The peak absorption is concentrated between 8.86 and 10.0

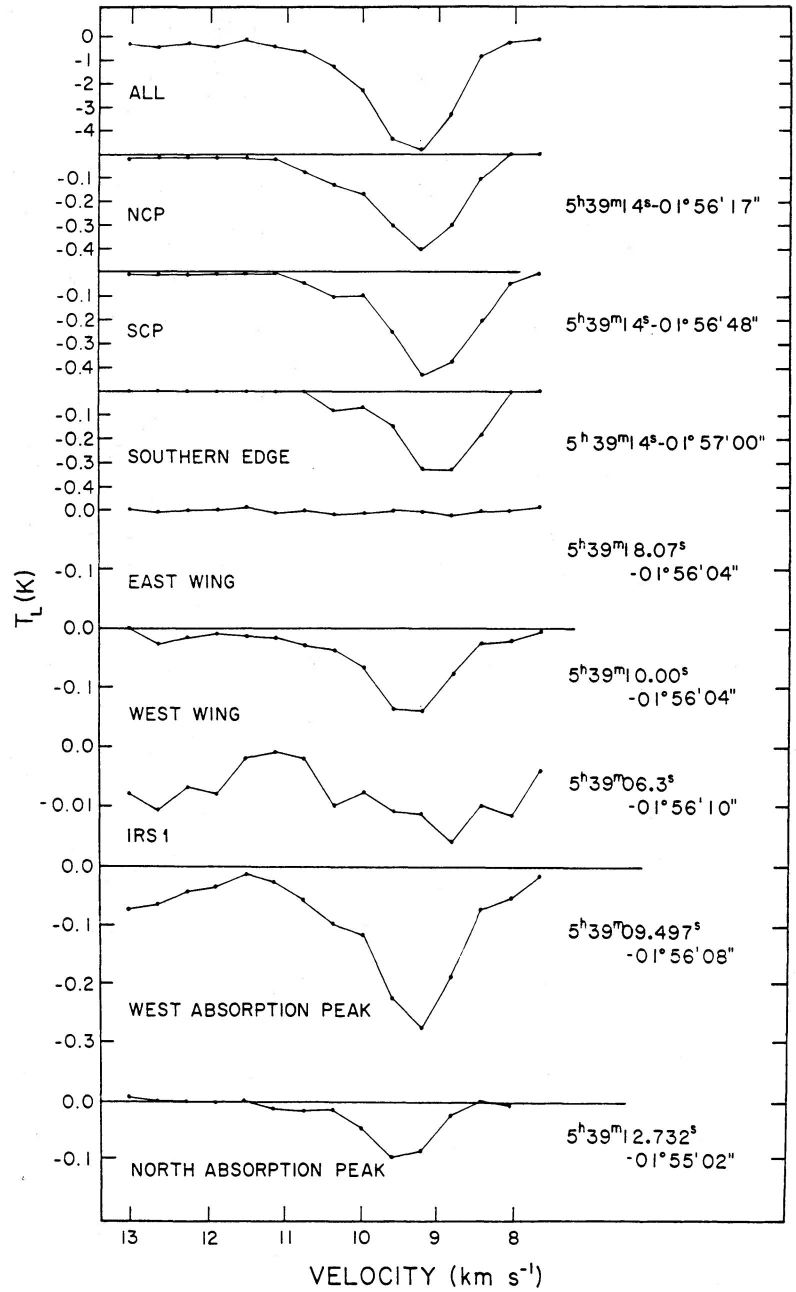

FIG. 2.—The absorption spectrum of H_2CO obtained at different points in NGC 2024. The LSR radial velocity is given in km s^{-1} while the line depth is given in flux density. The spectrum marked ALL is the average spectrum obtained over a 7′ × 7′ box centered on $\alpha_{1950} = 5^h39^m15^s$, $\delta_{1950} = -01°56'$. For all other spectra, the flux density has been summed over a 20″ × 20″ region centered on the position given. Note that the deepest absorption feature shifts from ~9.3 km s^{-1} to 9.7 km s^{-1} going north from the SCP.

km s^{-1}. The line optical depth $\tau = \ln(T_c/|T_L|)$, where $|T_L|$ is the absolute value of the brightness temperature of the line maps and T_c is the continuum brightness temperature. Seven of the H_2CO optical depth maps are displayed in Figure 3; these contain all of the significant H_2CO absorption. Each map is labeled in the lower left corner by the radial velocity in km s^{-1} with respect to the local standard of rest. The continuum map has not been corrected for the missing flux density. Each optical depth map is cut off at the 10% continuum contour, which defines the boundary of our optical depth maps. Because of the missing continuum intensities, the optical depths are upper limits. Close to the boundary of our maps the value of τ could be a factor of 2 too large. Maps with complex optical depth distributions have had the contours labeled by 10 times the optical depth of selected contours. All closed contours enclose peaks except those with inner tick marks. The lowest τ contour displayed is 0.2, and the increment is 0.2. The highest contour plotted is that for an optical depth of 1.0. However, the maps at velocities of 8.86, 9.24, and 9.62 km s^{-1} all have optical depths as high as 4 within the $\tau = 1.0$ optical depth contours. Such high optical depths occur over very small areas at the extreme north and south of the maps; because of the low

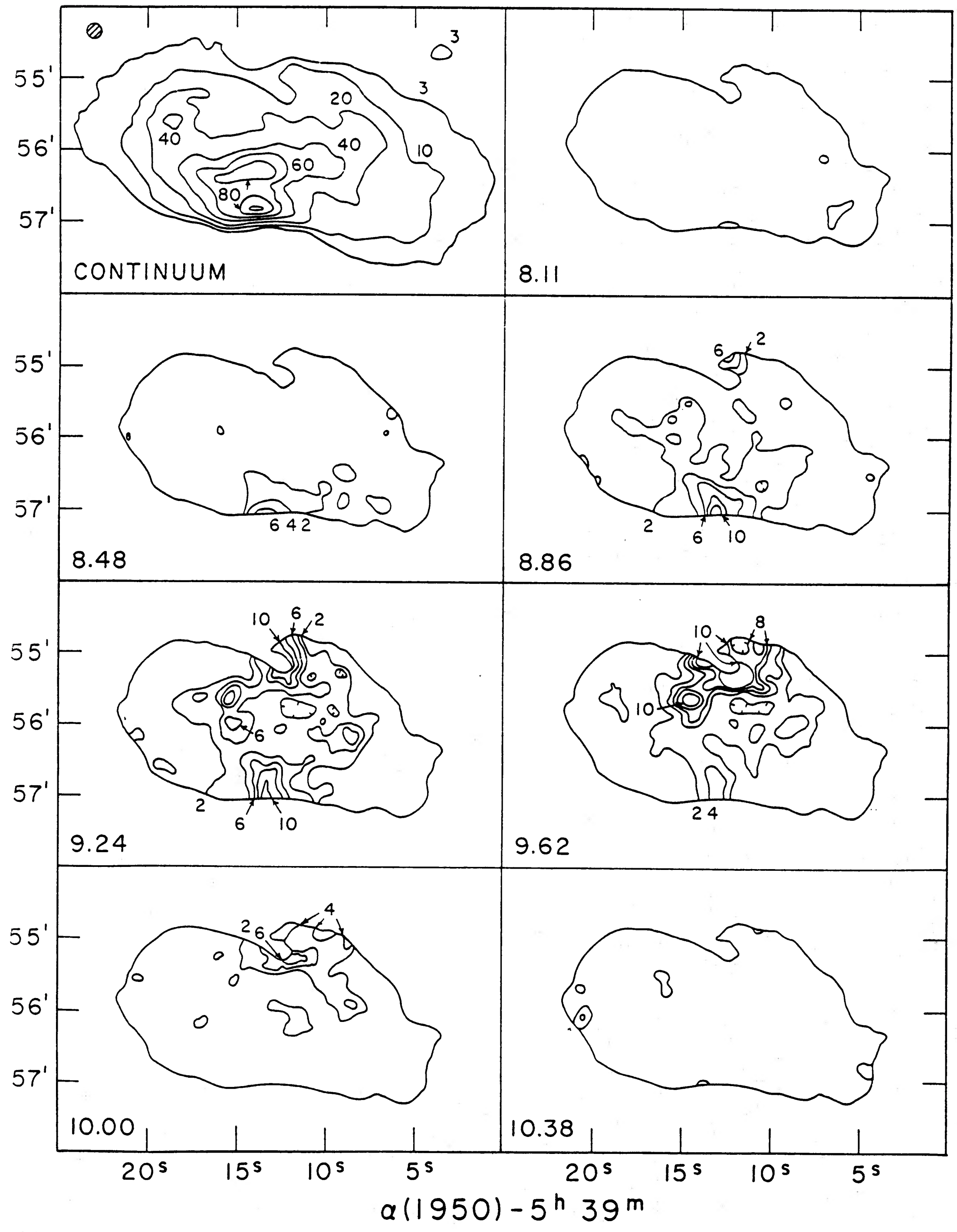

FIG. 3.—Maps of the continuum and of the apparent optical depth of the H_2CO 6 cm line toward NGC 2024. Contours are labeled by 10 times the optical depth. LSR radial velocities (km s^{-1}) are given in the lower left corner of each map.

continuum intensities there, the H_2CO optical depths are overestimated. Adding the missing single-dish flux density reduces τ by a factor of 2. Still, theses values are indistinguishable from infinity.

Most of the H_2CO absorption shown in Figure 3 occurs at 9.24 km s^{-1} and the adjacent velocity channels. At 8.86 km s^{-1} the peak optical depth at the southern edge is 1.9 (which is not definitely distinguishable from infinity since it occurs right at the 10% continuum level). The absorption has spread over a considerable area to the north in the form of two "fingers" extending northeast and northwest. Significant absorption also appears to the extreme north. The map for 9.24 km s^{-1} shows the H_2CO distribution at the velocity of maximum absorption integrated over the maps, i.e., at the center of the H_2CO absorption line. If one uses the 0.6 contour of optical depth as a tracer of high absorption, the following picture emerges. At the northern and southern extremities of the map, the east-west width of the absorption is ~0'.4. About

0'.5 inside of the north and south map boundaries (defined by the 10% continuum contour), the H_2CO contours bifurcate and form a ring with a radius of $\sim$0'.9 about the center of the 10% continuum contour. The relative minimum slightly to the north of the center of this molecular ring corresponds to an optical depth of $\sim$0.1. At 9.62 km s^{-1}, H_2CO absorption is concentrated to the north. This map resembles a mirror image of the 8.86 km s^{-1} map, with a bifurcation developing from the north rather than from the south.

Since the H_2CO line has six hyperfine components spread over 30 kHz, or 1.8 km s^{-1} (see Tucker, Tomasevich, and Thaddeus 1971 for frequencies and relative intensities), there is some blending of the velocity structure. For example, the weak absorption near the SCP at 10.38 km s^{-1} is probably not due to gas at that velocity, but rather to absorption in the $F = 1 - 0$ hyperfine component at a velocity near 9.24 km s^{-1}. Similarly, the apparent absorption at 8.86 km s^{-1} in the extreme north is probably due to $F = 1 - 1$ component absorption in gas at a velocity near 9.62 km s^{-1}. Hence, the real velocity gradient pattern from south to north is probably significantly cleaner than is apparent in Figures 2 and 3. The hyperfine structure does allow us to place limits on the maximum H_2CO optical depths at the extreme north and south positions where signal-to-noise considerations do not allow high optical depths to be distinguished from infinity. If the optical depths mentioned in the above examples are due entirely to weak hyperfine-component absorption, the maximum optical depths are $\sim$5 and 10 at the extreme southern and northern positions, respectively.

Figures 4 and 5 display a subset of the continuum and H_2CO contours on an optical photograph of the region. Figure 4 shows the 60% and the 3% continuum contours from Figure 3. The 60% contour defines the inner core of the H II region. Clearly, most of the activity is near the center of the dark bar of dust which extends primarily north-south. The lower contour defines the area over which we can map the extended radio H II region. The optical image of the H II region shows that the ionized gas extends considerably beyond the lowest radio contour, particularly to the north, east, and west. The optical image of the H II (particularly on prints with less contrast, so that details within the optically observed H II are seen) shows the same apparent morphology as does the radio map, with filaments sweeping east and west out of the dark bar and then turning northward.

Figure 5 shows the 0.2 contour of H_2CO optical depth from the 9.24 km s^{-1} map of Figure 3. The H_2CO appears to follow the dark bar almost perfectly. Remembering that the open ends of the contours to the north and south may be due only to an inadequate radio continuum level to define optical depths, one hypothesizes that the contours would extend farther to the north and south and outline the dark lane. The H_2CO absorption appears to trace out a ring, as discussed above. This ring is completely invisible optically, but there is a dust filament to the east and then to the northeast just where the H_2CO ring has its maximum extent eastward. The two small "cloudlets" to the east of the bar defined by 0.2 optical depth contours seem to correspond to knots or patches in the dust distribution.

f) H_2 *Density and Isotope Corrections*

Henkel, Walmsley, and Wilson (1980) determined that the H_2 density, $n(H_2)$, is $10^{4.9}$ cm^{-3} from the 2_{11}–2_{12} (2 cm) and 1_{10}–1_{11} absorption line of H_2CO. This value of $n(H_2)$ is averaged over the 2'.6 beam used and depends on the value of optical depth in the 1_{10}–1_{11} line. Henkel *et al.* (1980) took the apparent optical depth as 0.28; using our median value of τ in the 9.3 km s^{-1} channel, 0.21, we also obtain $n(H_2) = 10^{4.9}$ cm^{-3}. This value is at least a factor of 3 uncertain, from the difference between slab and spherical cloud geometries. Because of the complex structure of the H_2CO absorption, cloud sizes are at best qualitative. We estimate that the characteristic size would be $\sim$0'.5 from the τ maps. Using this size and the column density of ortho–H_2CO, 2.5×10^{13} cm^{-3}, we obtain a H_2CO space density of $\sim 10^{-4}$ cm^{-3}. If the H_2 density is $\sim 10^5$ cm^{-3}, we obtain an (ortho–H_2CO/H_2) ratio of $\sim 10^{-9}$.

The isotope ratios from the 1_{10}–1_{11} line must be corrected for photon trapping (see, e.g., Henkel, Walmsley, and Wilson (1980). The correction depends on both τ and $n(H_2)$. Using our median value of τ, the value of $n(H_2)$ and the measurements of Henkel, Wilson, and Bieging (1982), we have a ($H_2CO/H_2{}^{13}CO$) ratio of $\sim 70 \pm 11$.

g) *Maps of Emission-Line Molecules*

Snell *et al.* (1983) have carried out a multitransition study of NGC 2024 in millimeter-wavelength lines of CS. In order to derive the column density of CS and the density of the H_2 which collisionally excites the CS, they carried out a large velocity-gradient radiative transfer analysis of their multitransition data. They found that $n(H_2)$ is $10^{6.2}$ cm^{-3} near $\alpha_{1950} = 05^h39^m13^s$, $\delta_{1950} = -01°56'7''$. The H_2 density decreases by a factor of $\sim$3 within 2'–3' of this position in all directions. The column density of CS has a maximum near the position of maximum $n(H_2)$ and decreases by a factor of 10 within $\sim$2' east and west and within $\sim$4' north and south of the peak position. The radial velocity of the CS lines is essentially constant at 10.5 km s^{-1}, which is $\sim$1.2 km s^{-1} higher than the H_2CO peak. From the location and difference in radial velocity between CS emission and H_2CO absorption, the CS is probably located behind the H II region.

Johnston, Sloanaker, and Bologna (1973) reported the discovery of a weak H_2O maser toward NGC 2024 with a velocity near 11 km s^{-1}. Genzel and Downes (1977) reobserved this maser and reported a velocity of 10 km s^{-1}; they determined the position of the maser with an uncertainty of 6'': $\alpha_{1950} = 05^h39^m13^s.7$, $\delta_{1950} = -01°57'30''$.

IV. DISCUSSION

In Figure 6 we have plotted contours representing the distributions of the ionized gas, molecular gas and hot dust, two at a time. The infrared contours, representing the distribution of hot dust, are taken from Grasdalen's (1974) 8.4 μm map. The H_2CO contours are an average of the maps at 8.86, 9.24, and 9.62 km s^{-1}; the contours are labeled in optical depth times 10. The H II contours are from the same continuum map as used to produce Figure 3. The bottom panel of Figure 6 compares the distribution of the foreground molecular gas, as shown by H_2CO, and the ionized gas. The southern compact H II region is just to the northeast of the H_2CO peak. The east-west extension of the northern compact H II region appears to bisect the two peaks of the H_2CO absorption. The middle panel compares the distribution of the hot dust and the molecular gas seen in front of the radio continuum. The peak of the infrared emission is nearly coincident with the southern peak of H_2CO optical depth. The top panel of Figure 6 compares the radio continuum and the IR. The ridge of the 8.4 μm infrared contours follows the 5% continuum contour nearly

FIG. 4.—The 60% and 3% continuum contours on an optical photograph of NGC 2024

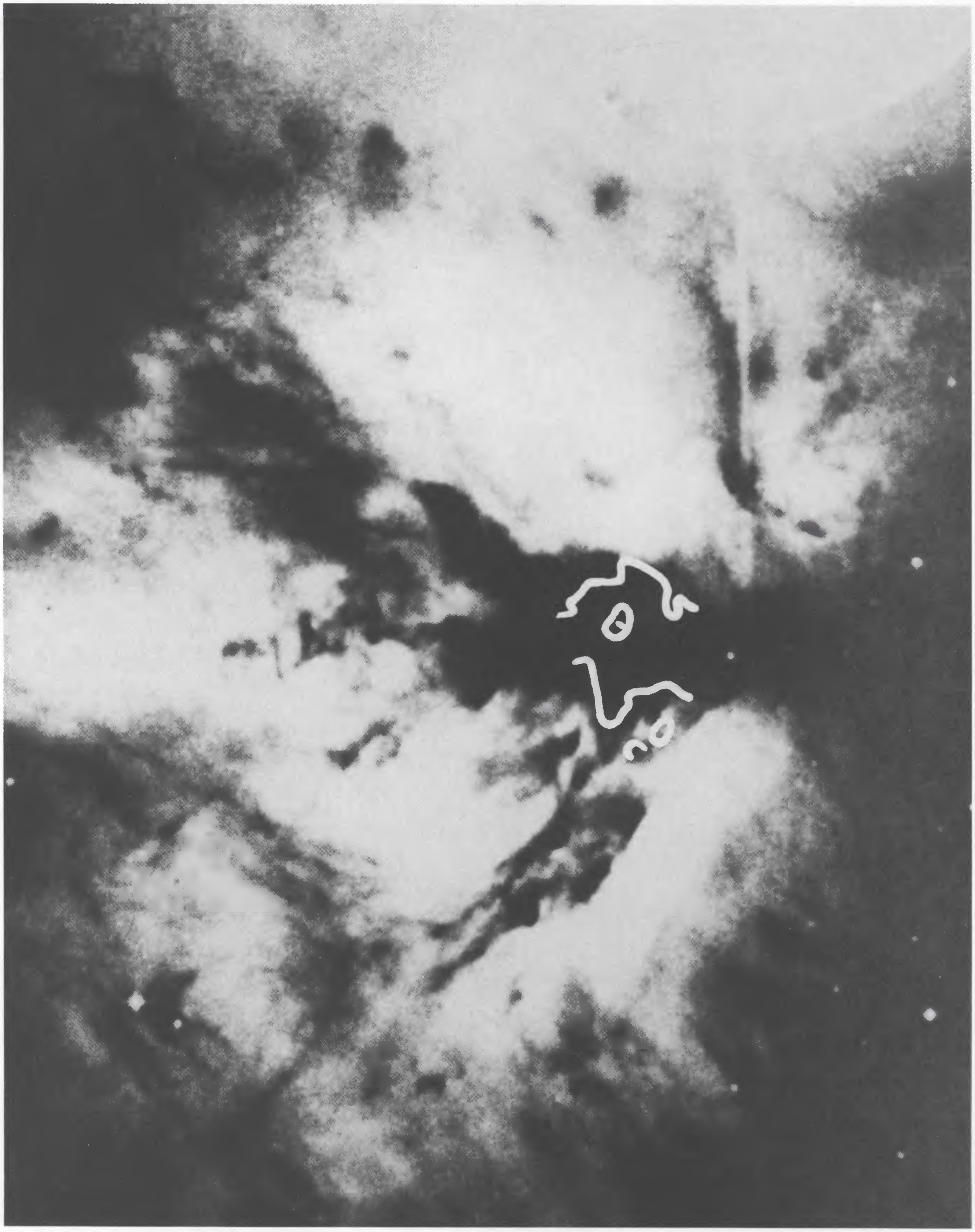

FIG. 5.—The 0.2 optical depth contour for the average of channels at 8.86, 9.24, and 9.62 km s^{-1} on an optical photograph of NGC 2024

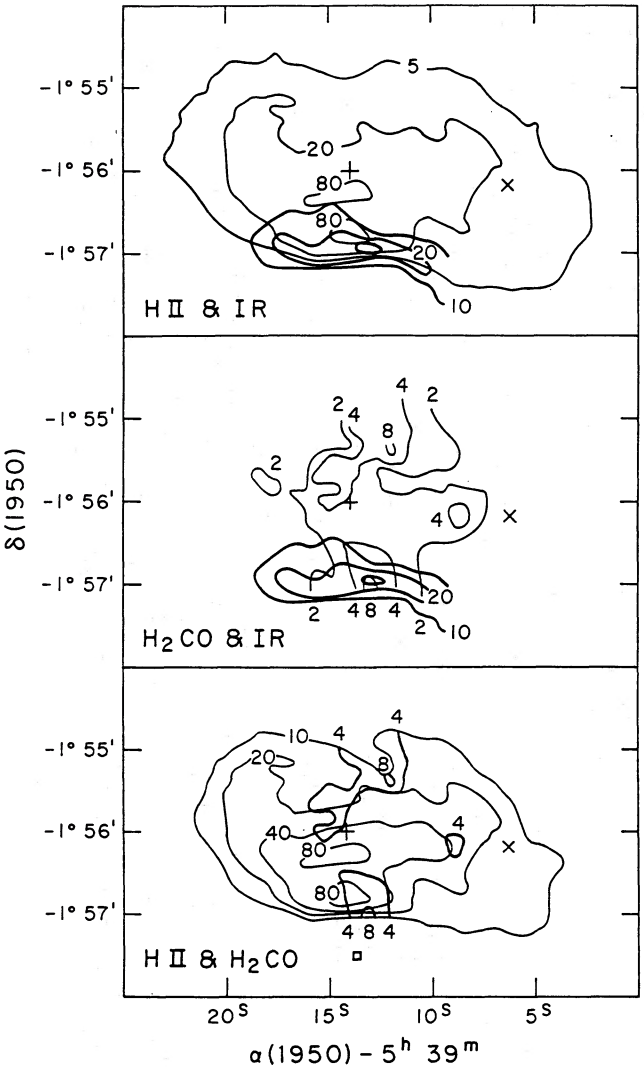

FIG. 6.—Comparison of the distribution of H II (our VLA continuum map), hot dust (Grasdalen's 8.4 μm map), and molecular gas in absorption (our VLA 9.24 km s^{-1} H_2CO optical depth map). The plus sign (+) and cross (×) mark the positions of IRS 1 and IRS 2.

perfectly, and the peak of the infrared emission lies just to the southwest of the peak of the southern compact H II region.

a) A Model for NGC 2024

The study of Snell *et al.* (1983) showed that the core of the molecular cloud has an H_2 density of $\sim 10^{6.2}$ cm^{-3}. The radial velocity of this dense gas, 10.5 km s^{-1}, does not change along the north-south line through the SCP. Since significant molecular absorption is not seen at velocities greater than 10 km s^{-1}, we infer that the core of the cloud lies behind the H II region. In contrast, most of the H_2CO is located in regions where $n(H_2)$ is 10^5 cm^{-3} (which may not be significantly different from 10^6 cm^{-3}). The radial velocity is $\sim$9.3 km s^{-1}. Hence, the molecular ring seen in H_2CO on the plane of the sky appears to be a three-dimensional bubble, with the molecular gas detected by H_2CO–line absorption of the H II radio continuum expanding toward us while the back of the bubble remains essentially unaffected. From the difference in molecular line velocities, the expansion velocity would be $\sim$0.6 km s^{-1}.

The fact that the southern edge of the radio continuum is unresolved on our VLA map suggests strongly that the H II region is sharply ionization bounded to the south because of a very high gas density just south of the SCP. The sharp increase in the H_2CO optical depths just to the south of the SCP provides support for this suggestion. If S3 is of spectral type O9 zero-age main sequence (ZAMS) and the density of the molecular gas to the south is 10^6 cm^{-3}, the flux of ionizing photons would penetrate only $\sim 10^{16}$ cm (2″) into the dense gas. Photons which do not have sufficient energy to ionize hydrogen could penetrate only a short distance into the very dense molecular gas and dust, heating the dust and leading to the strong extended infrared emission centered 1×10^{17} cm southwest of the SCP. It is to be expected that the hottest dust lies close to the source of the heating in the SCP, i.e., in the very dense molecular gas just south of the ionization front. Thus, the shape of the extended 8.4 μm emission is very extended east-west and very narrow north-south. At longer wavelengths (see, e.g., far-infrared (FIR) maps of Thronson *et al.* 1984) the cooler dust located farther from the heating source dominates the infrared emission, which becomes more nearly circular in shape. The strong carbon recombination-line emission which comes from near the peak of the extended 8.4 μm emission is the result of carbon-ionizing photons penetrating southward beyond the hydrogen ionization front.

The H II region expands freely northward into the much lower density volume inside the molecular bubble. The decrease in the electron temperatures reported by Krügel *et al.* (1982) could be related to lower electron densities in the H II region. The very dense molecular gas located behind the H II region prevents the H II from expanding in this direction, so the expansion is constrained to be in the directions toward the Sun and to the north, east, and west. All radial velocities of the hydrogen recombination lines are more negative than the velocity of the dense molecular cloud. The closest agreement in the velocities of the H II and the molecular gas comes at the ionization front near the SCP, where there is very little expansion toward the Sun. As one looks farther north of the ionization front, a larger fraction of the H II is expanding toward us.

Most of the extended radio emission appears to be associated with the extensions of the northern compact H II region. The map suggests that as ionized hydrogen expands northward from the ionization front, it is constrained from flowing smoothly past the position of IRS 2. Instead, there is an apparent pileup of H II in the northern compact H II region, which is located just south of IRS 2. The ionized hydrogen then may flow around IRS 2. This pileup may be due to an interaction between the H II flow and the stellar wind from IRS 2 (which is deduced to exist from the presence of very broad and localized Bγ emission at the position of IRS 2). If so, the northern compact H II region would then be the position where the stellar wind and the northward expansion of H II from the ionization front are in pressure equilibrium.

Black and Willner (1984) suggest that IRS 2 is a Be star, based on the lack of a $^2P_1$ helium line indicating a low stellar surface temperature. If so, IRS 2 cannot be the star which provides the excitation of NGC 2024. The extinction deduced from the Brackett-series lines, 12 magnitudes, might be larger if the circumstellar H II region of IRS 2 is optically thick. All of the hydrogen-ionizing photons from IRS 2 would be used up in the production of this dense, optically thick circumstellar H II region. Employing the formulation of Simon *et al.* (1983), we find $\dot{M} \approx 4 \times 10^{-7}$ $M_\odot$ yr^{-1}, which agrees with the esti-

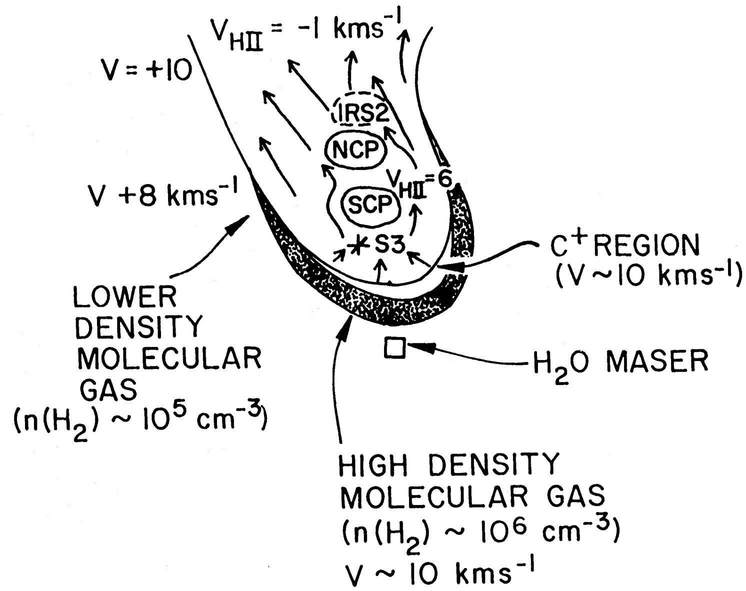

FIG. 7.—A schematic diagram of the gas in the NGC 2024 region. The (proposed) exciting star, S3, lies just south of the SCP and NCP. This H II region outlines a molecular bubble which is centered close to IRS 2. The region centered on S3 has a high density $n_{H_2} = 10^6$ and a velocity of 10 km s^{-1}. It is here that the strong continuum IR emission originates. Going northward along the bubble, the ionized gas expands to the northwest and northeast edge of the bubble, causing the density to decrease to $n \approx 10^5$.

mate given by Black and Willner (1983). The predicted radio flux at 6 cm of ~ 3 mJy is undetectable on our VLA map, because of the confusion with the extended ionized material.

In this interpretation, the northern compact H II region will not be a stable structure and therefore would be very young. If IRS 2 originally created the molecular bubble and S3 was originally buried in the dense molecular cloud to the south, the H II region surrounding S3 may only recently have broken through into the molecular bubble. Hence, if the northward expansion of H II from the ionization front south of S3 toward IRS 2 is a recent phenomenon, the instability of the pileup of H II in the northern compact H II region may not be apparent at the angular resolution of our VLA data. An age of order 10^5 yr for the present structure of the radio continuum is consistent with the observed distribution and kinematics of the ionized hydrogen.

Finally, the H_2O maser south of the ionization front and at the velocity of the undisturbed, dense molecular cloud may indicate that star formation is now going on to the south of the ionization front. Another signpost of continuing star formation activity to the south of the ionization front is the detection by Sanders and Willner (1985) of a bipolar outflow centered $\sim 30''$ southwest of the H_2O maser position. They also detected a new infrared source near this position, which cannot, however, be S3 since it is $\sim 1'$ south of the ionization front. The proposed model is schematically illustrated in Figure 7.

b) A Scenario for the History of NGC 2024

A possible history of NGC 2024 is the following. Star formation in the original dense molecular cloud began on the side closer to the Sun, and the newly formed stars began to blow a bubble in the surrounding molecular gas. Because the densest region of the molecular cloud is behind the region of star formation, the ionized hydrogen in the molecular bubble broke through the molecular cloud on the side toward the Sun and to the east and west of the north-south elongated cloud. IRS 2 may have been the dominant agent in the early stages of the formation of the bubble. Star formation activity proceeded in time southward. S3 formed from the dense molecular cloud and initially produced an H II region which may have been separated from the cavity surrounding IRS 2. Eventually, the expanding compact H II region surrounding S3 broke through into the cavity. Ionized hydrogen now expands off the ionization front to the south of S3 toward IRS 2. IRS 2 is an early B star surrounded by a dense, optically thick circumstellar H II region formed by a radiation-driven stellar wind. IRS 2 does not ionize the molecular gas in the surrounding molecular bubble because its Lyman photons cannot escape this circumstellar region. At the position south of IRS 2 where this stellar wind and the H II expanding northward are in pressure equilibrium, there is a pileup of ionized hydrogen. The H II flows around IRS 2 and escapes from the cavity through holes in the molecular bubble. The H_2O maser south of S3 is a signpost of continuing star formation deep within the molecular cloud.

R. M. C. acknowledges with thanks support from NSF grants AST 81-14887 and AST 85-03387. C. H. thanks the Bell Telephone Laboratory for their hospitality during his stay there.

REFERENCES

Bieging, J. H., Wilson, T. L., and Downes, D. 1982, *Astr. Ap. Suppl.*, **49**, 607.
Black, J. H., and Willner, S. P. 1984, *Ap. J.*, **279**, 673.
Crutcher, R. M., and Hall, D. N. B. 1983, private communication.
Frey, A., Lemke, D., Thum, C., and Fahrback, U. 1979, *Astr. Ap.*, **74**, 133.
Garrison, R. F. 1968, *Pub. A.S.P.*, **80**, 20.
Genzel, R., and Downes, D. 1977, *Astr. Ap. Suppl.*, **30**, 145.
Grasdalen, G. L. 1974, *Ap. J.*, **193**, 373.
Henkel, C., Walmsley, C. M., and Wilson, T. L. 1980, *Astr. Ap.*, **109**, 344.
Henkel, C., Wilson, T. L., and Bieging, J. H. 1982, *Astr. Ap.*, **109**, 344.
Johnston, K. J., Sloanaker, R. M., and Bologna, J. M. 1973, *Ap. J.*, **182**, 67.
Krügel, E., Thum, C., Martin-Pintado, J., and Pankonin, V. 1982, *Astr. Ap. Suppl.*, **48**, 345.

Löbert, W., and Goss, W. M. 1978, *M.N.R.A.S.*, **183**, 119.
Sanders, D. B., and Willner, S. P. 1985, *Ap. J.* (*Letters*), **293**, L39.
Simon, M., Felli, M., Cassar, L., Fischer, J., and Massi, M. 1983, *Ap. J.*, **266**, 623.
Snell, R. L., Mundy, L. G., Goldsmith, P. F., Evans, N. J., II, and Erickson, N. R. 1984, *Ap. J.*, **276**, 625.
Thompson, R. I., Thronson, H. A., Jr., and Campbell, B. G., 1981, *Ap. J.*, **249**, 622.
Thronson, H. A., Jr., Lada, C. J., Schwartz, P. R., Smith, H. A., Smith, J., Glaccum, W., Harper, D. A., and Lowenstein, R. F. 1984, *Ap. J.*, **280**, 154.
Tucker, K. D., Tomasevich, G. R., and Thaddeus, P. 1971, *Ap. J.*, **169**, 429.

J. H. Bieging: Radio Astronomy Laboratory, University of California, 601 Campbell Hall, Berkeley, CA 94720

R. M. Crutcher: Astronomy Department, University of Illinois, 349 Astronomy Building, 1011 West Springfield Avenue, Urbana, IL 61801

C. Henkel and T. L. Wilson: Max-Planck-Institut für Radioastronomie, Auf Dem Huegel 69, Bonn, West Germany

K. J. Johnston: Code 4130, E. O. Hulbert Center for Space Research, Naval Research Laboratory, Washington, DC 20375